Applied Acoustics 221 (2024) 110000

Contents lists available at ScienceDirect

Applied Acoustics

journal homepage: www.elsevier.com/locate/apacoust

Geometric optimisation of a multiple coiled-up resonator for broadband and octave band acoustic absorption

Cristina Marescotti *, Francesco Pompoli *

Department of Engineering, University of Ferrara, Via Saragat 1, Ferrara 44121, Italy

ARTICLE INFO

Keywords:
Coiled quarter-wave resonators
Acoustic metamaterials
Broadband absorption

ABSTRACT

This study presents a comprehensive approach to designing sound absorption metamaterials, aiming to achieve broadband absorption capabilities while maintaining a compact thickness, starting from an exceptionally low frequency of 100 Hz. By employing a parallel arrangement of resonators with varying lengths, the proposed approach exploits the envelopes of absorption frequencies to realize broad-spectrum sound absorption.

An analytical model is utilized in the geometric optimization phase, accounting for inlet losses and thermo-viscous losses near the walls. The absorption for multiple ducts coupled in parallel is derived using the series and parallel impedance method. A geometric parameterization procedure is implemented to maximize normal incidence acoustic absorption, leading to design optimization for both broadband and octave-band absorbers. Design maps are established to assess acoustic performance and physical space requirements, facilitating informed decision-making in metamaterial design.

Prototype fabrication and experimental validation involve 3D printing of optimized geometries using poly-lactic acid, followed by testing within impedance tubes according to ISO 10534–2 standards. The results demonstrate the effectiveness of the proposed method in achieving broadband sound absorption across specified frequency ranges.

1. Introduction

Low-frequency sound attenuation is currently garnering significant interest for various reasons. Low-frequency noise not only contributes to health problems but also poses challenges in attenuation due to the intrinsic loss mechanisms of conventional sound-absorbing materials [1]. Conventional sound absorption methods can be categorised into two main types: porous and fibrous sound absorption materials, and resonant sound absorption materials. Porous materials are well-described by propagation models and generally perform well in the mid- and high-frequency ranges but exhibit inefficiency at low frequencies [1,2]. Achieving better absorption performance with porous materials often requires increased thickness, which limits their potential applications. On the other hand, resonant absorption materials such as Helmholtz resonators [3–7], micro-perforated panels [8–10], and coiled-up channels [11–15] demonstrate excellent absorption performance in the mid- to low-frequency range due to vibration resonance effects, but they have narrow bandwidth absorption.

In the past decade, researchers have explored various absorption strategies to achieve broadband absorption, aiming to combine excellent low-frequency absorption with limited thickness. To effectively address the challenge of low-frequency noise, numerous studies have investigated different approaches. For example, optimising micro-perforated panels (MPP) can enhance their sound absorption performance [13,16]. Additionally, various types of acoustic metamaterials have emerged, including locally resonant sonic crystals [17,18], decorated membranes [19,20], split tubes [21,22], quarter-wave resonators [23–25], and Helmholtz resonators (HR) with extended and spiral necks [3–5], among others. These materials possess periodic structures and thicknesses smaller than the wavelength of the incident acoustic wave, with their acoustic characteristics primarily determined by geometry rather than the base material. However, as the sound absorption performance of these metamaterials primarily relies on resonance, they operate within a narrow frequency range centred around their resonant frequency, significantly limiting their applicability.

Recent works have proposed solutions to achieve broadband absorption by introducing multiple absorbers with different peaks. For instance, Peng et al. [26] introduced a honeycomb composite subsurface

* Corresponding authors.
E-mail addresses: mrscst@unife.it (C. Marescotti), pmpfnc@unife.it (F. Pompoli).

https://doi.org/10.1016/j.apacoust.2024.110000
Received 23 November 2023; Received in revised form 22 February 2024; Accepted 26 March 2024
Available online 30 March 2024

plate with a sound absorption rate of 90 % and a thickness of less than 30 mm in the range of [600 – 1000] Hz. Yingli Li et al. [27] proposed multiscale porous material with coiled-up channels and employed a parallel-coupling method to achieve broadband absorption at low frequencies, exceeding 50 % above the range of [211 – 3000] Hz, with a subwavelength dimension of 1/16. Yipu Wang et al. [28] proposed a coupled structure of four coiled-up space cores embedded in a porous material (CSPMs), which achieved over 75 % sound absorption performance within the frequency range of [195 – 600] Hz. Therefore, it appears necessary to combine different material types or employ parallel or series configurations of different resonators [12,29] to achieve effective broadband sound absorption.

Building upon these previous works, this study proposes a geometric optimisation procedure for sound absorption metamaterials, based on the appropriate sizing of parallel-coupled quarter-wave resonators. In addition to this, the objective is to develop an innovative system that does not require the use of distinct materials, for example CSPM system, but rather depends solely on the precise sizing of these resonators, starting from a remarkably low frequency (100 Hz). A quarter-wave resonator consists of a closed-ended tube that generates a resonant standing wave at the fundamental frequency and odd harmonics. The resonance frequencies of the system are solely determined by the tube length according to the theoretical formula:

$$f_{res} \cong \frac{c_0(2n-1)}{4l}, \tag{1}$$

where c_0 is the sound speed of the fluid inside the resonator and $n = 1, 2, 3\cdots$ indicates the number of harmonics [30]. The acoustic behaviour of the coiled-up resonator is governed by two primary loss mechanisms: thermal loss, primarily caused by heat diffusion from the sound field at the boundaries, and viscosity loss, which occurs when the fluid experiences friction at the boundaries. Additionally, while the length of the tube determines the resonance frequencies, dissipative phenomena play a crucial role in determining the amplitude of the absorption peaks relative to the frequency and system porosity [31,32]. These phenomena remain significant even in broadband multifrequency systems since the envelope of the resonance peak curve strongly depends on dissipation. The analytical model detailed earlier has been substantiated through experimental validation, as outlined in reference [33] and discussed in depth in the referenced article [30]. The validation process covered both single resonator scenarios and configurations involving a parallel coupling of resonators.

Therefore, in the initial phase of this study, this model was utilised to forecast the absorption profile of the coiled-up metamaterial, both for individual resonators and for resonators coupled in parallel. This model encompasses the definition of radiation impedances arising from surface irregularities, inlet hole losses, and the visco-thermal theoretical formulations along the resonator path, as previously described [30]. Upon detailing the analytical model and the various metamaterials obtained (both broadband and octave band absorbers), the entire analytical process will be examined from a broader standpoint. The overarching objective is to create investigative tools to aid the design of these sound-absorbing systems.

Via a geometric optimisation process, a configuration comprising nine parallel-coupled straight tubes, each of varying lengths, was developed. The objective was to maximise broadband sound absorption, spanning from a minimum frequency of 100 Hz to higher frequencies. Additionally, apart from the broadband metamaterial, the sizing of the absorbers targeting specific octave bands will be presented. These specialised systems are optimised to absorb sound within distinct octave bands, demonstrating enhanced efficiency compared to the broadband absorbers as they necessitate fewer resonators to achieve higher efficiency. Specifically, two absorbers designed for octave bands of 125 Hz and 250 Hz will be shown.

Upon completing the simulation of the optimal geometry, 3D samples were produced through 3D printing using plastic (PLA) material. In order to evaluate the authentic acoustic behaviour of the metamaterial, an impedance square section tube was devised and manufactured. This experimental setup aims to corroborate the findings from simulations and provide tangible evidence for the efficiency of the designed metamaterial.

2. Theoretical analysis: Analytical model

To accurately predict the acoustic behaviour of the investigated metamaterial, an analytical model was developed to determine the acoustic absorption coefficient at normal incidence. This was achieved by modifying the key geometric parameters of the coiled-up quarter-wave resonators. The analysis began by examining the different contributions of acoustic losses, and visco-thermal loss models [34] were employed to define sound absorption in narrow tubes. In such structures, energy loss due to viscosity and thermal conduction plays a significant role in determining absorption. These losses occur within the viscous and thermal boundary layers near the walls of the duct. When the cross-sectional dimensions of the acoustic domain are much larger than the thickness of the boundary layer, the influence of visco-thermal loss is mainly confined to the boundary layer [35]. It is important to underline that in all studies on the acoustic propagation of ducts the surface roughness is not considered, since in the hypothesis of linear acoustics the laminar fluid dynamic regime is assumed and in this case the friction factor is independent of this parameter.

For a comprehensive theoretical discussion on the acoustic losses generated within the ducts and their impact on the acoustic behaviour of these resonators, please refer to a previously published article [30], which outlines all the steps and assumptions made in defining the analytical model. However, a brief overview of the analytical model employed for the acoustic modelling of the individual resonators and their subsequent parallel coupling will be provided.

The sound-absorbing metamaterial under investigation consists of a coiled-up quarter-wave resonator, as depicted in Fig. 1a. The system comprises an “inlet” region characterised by a square-section hole with a side length of d and a thickness of l_{inlet}. It also includes a coiled-up quarter-wave tube with a length of l and a front mask to facilitate positioning of the resonator within the measurement setup. Fig. 1a illustrates the adapter used for normal incidence sound absorption measurements [33], which were conducted in an impedance tube with a diameter of $D = 45.0$ mm. Additionally, square-section quarter-wave resonators were chosen to simplify the fabrication process using a 3D printer, compared to using circular cross-sections.

Certain aspects within the analytical model were not considered; specifically, the coiled-up tubes were treated as straight tubes, and no corrections were made, neglecting their curvature. Indeed, finite element simulations were conducted using a model previously validated through experimental measurements [36]. These simulations demonstrated that the comparison between rectilinear and curvilinear ducts does not result in changes in the sound absorption coefficient for normal incidence. This is illustrated in Fig. 2a, where the trends are compared for both the analytical AM model (solid red line) and the two simulations for rectilinear (dashed black line) and curvilinear (dotted blue line) configurations. Additionally, Fig. 2 displays the simulated geometries: Fig. 2b illustrates the FEM-simulated rectilinear geometry, while Fig. 2c depicts the FEM-simulated coiled-up geometry. Both figures display the impedance tube (yellow volume), where the sound field develops and the sound pressure is measured in accordance with the standard [33], and the two simulated ducts (blue volumes).

The inlet hole is modelled as a dissipative fluid to account for energy losses resulting from the narrowing of the section. Similar to the case of perforated panels [37–41], a dissipative fluid is introduced inside the hole using the well-known Johnson-Champoux-Allard (JCA) model. This allows the resonant systems to be modelled by assigning complex properties of sound speed and density that depend on appropriate physical parameters. These properties capture the losses near the inlet

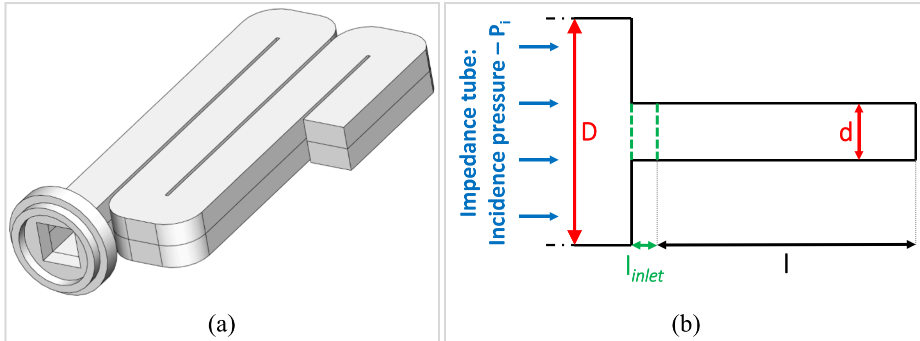

Fig. 1. (a) A 3D sound absorption coiled quarter-wave resonator, (b) diagram of a straight tube with all the main geometric quantities.

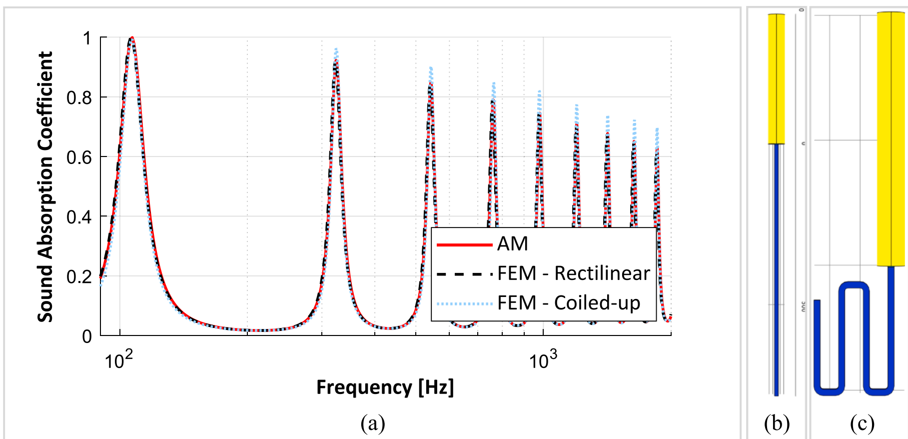

Fig. 2. Comparison of analytical model (AM) and numerical model (FEM): straight duct (b) and coiled duct (c).

due to the sudden variation in the section where the acoustic wave interacts with the perforated surface. The JCA model requires five descriptive physical parameters, which are dependent on the geometry of the duct:

- Airflow resistivity σ: this represents the ratio of the real resistive part of the hole surface impedance to its thickness [37–39]. The airflow resistivity is a combination of two resistive terms: one accounting for the viscous effects within the hole and the other representing dissipation at the edges due to the distortion of the acoustic flow. It is a function of the angular frequency ω and is related to the hole porosity ϕ and the unit cell perforation ratio ϕ_{sec}, which is the ratio of the cross-sectional area of the tube A_1 to the unit cell area A_{uc}. The specific airflow resistance R_s is calculated as $R_s = \frac{1}{2}\sqrt{2\eta\omega\rho_0}$, where η is the air dynamic viscosity and ρ_0 is the air density. The value of σ is divided by the unit cell perforation ratio ϕ_{sec}, taking into account the increase in flow velocity at the inlet hole due to the sudden change in cross section. A factor $\alpha_s = 4$ is empirically multiplied by the specific airflow resistance R_s to account for the viscous surface effects caused by sharp edges [41].
- Equivalent radius Λ and Λ': the parameters Λ and Λ' are equal to the equivalent radius r_{eq} of the hole, assuming the condition of straight cylindrical pores [30]. The equivalent radius r_{eq} is obtained by comparing the cross-sectional area of a circular tube with that of a square tube.
- Tortuosity α_∞: the tortuosity parameter α_∞ is set to 1.

Table 1 provides the most reliable expressions for the five parameters described above, which are required by the JCA model to predict the acoustic performance. In the remaining length l of the duct, the Low Reduced Frequency model (LRF) was employed to describe the sound wave propagation inside narrow tubes, considering the visco-thermal loss. According to the theory presented in the previous publication [30], the surface acoustic impedance at a specific point (1) inside the tube, beyond the inlet hole region, for the narrow tube with a rigid back wall as illustrated in Fig. 1, can be expressed as follows:

Table 1
JCA inlet hole parameters used in this formulation.

σ	Airflow resistivity	$\left[\left(\frac{2l_{inlet}}{r_{eq}}+1\right)\frac{\alpha_s R_s}{\phi}\frac{1}{l_{inlet}}\right]\frac{1}{\phi_{sec}}$	$\left[\frac{Pa\cdot s}{m^2}\right]$
ϕ	Porosity	1	[-]
α_∞	Tortuosity	1	[-]
Λ	Viscous characteristic length	r_{eq}	[m]
Λ'	Thermal characteristic length	r_{eq}	[m]

$$Z(1) = -jZ_{c1}cot(k_{c1}l_1) \tag{2}$$

where $Z_{c1} = \rho_{eff}c_{eff}$ is its effective impedance and $k_{c1} = \frac{\omega}{c_{eff}}$ is the effective complex wave number of the tube, ρ_{eff} the effective density that includes inertial and viscous contributions and c_{eff} the effective speed of sound and these quantities can be derived using the LRF model [30]. The surface acoustic impedance at the inlet hole (section 1_a), with reference to Fig. 1, can be derived as:

$$Z(1_a) = Z_{c1_{aJCA}}\frac{-jZ(1)cot\left(k_{c1_{aJCA}}l_{inlet}\right) + Z_{c1_{aJCA}}}{Z(1) - jZ_{c1_{aJCA}}cot\left(k_{c1_{aJCA}}l_{inlet}\right)}, \tag{3}$$

where $Z_{c1_{aJCA}} = \rho_{JCA}c_{JCA}$ and $k_{c1_{aJCA}} = \frac{\omega}{c_{JCA}}$, with $c_{JCA} = \sqrt{\frac{K_{JCA}}{\rho_{JCA}}}$ are respectively the effective impedance, the effective complex wave number of the inlet hole and the effective speed of sound, modelled as a porous substrate with the JCA model. The input surface acoustic impedance, which refers to the front section of the system, can be calculated as $Z_{in} = \frac{\left[\frac{Z(1_a)}{Z_0}\right]}{\phi_{sec}}$ [12] , and finally the normal incidence sound absorbing coefficient of the system is determined:

$$\alpha = \frac{4Re(Z_{in})}{|Z_{in}|^2 + 2Re(Z_{in}) + 1}, \tag{4}$$

where $Z_0 = \rho_0 c_0$ is the air specific acoustic impedance with the air density ρ_0 and the speed of sound c_0.

In the particular case of multiple coiled-up quarter-wave resonators of different tube lengths and the same cross-section assembled in parallel (Fig. 3b), the surface acoustic impedance can be obtained using the concept of the parallel equivalent circuit [42] as:

$$Z_{tot_{in}} = \left(\frac{\phi_{sec1}}{\left(\frac{Z(1_a)}{Z_0}\right)} + \frac{\phi_{sec2}}{\left(\frac{Z(2_a)}{Z_0}\right)} \right)^{-1}, \tag{5}$$

where $Z(1_a)$ and $Z(2_a)$ are the characteristic acoustic impedances at 1_a and 2_a for the tubes 1 and 2, and $\phi_{sec1} = \phi_{sec2}$ is the ratio between the cross-sectional area of tube 1 and 2. Furthermore, in this particular case, the unit cell perforation ratio, necessary to calculate the inlet hole effective parameters, will be given by $\phi_{sec} = \frac{N*A}{A_{uc}}$, where N is the number of identical tubes, and A the cross-sectional area of the single tube.

Then the absorption coefficient can be attained by:

$$\alpha = \frac{4Re(Z_{tot_{in}})}{|Z_{tot_{in}}|^2 + 2Re(Z_{tot_{in}}) + 1}, \tag{6}$$

When multiple quarter-wave resonators are coupled in parallel, additional considerations need to be taken into account regarding the overall effect. The absorption peaks in the frequency response correspond to the resonant frequencies of the individual quarter-wave resonators. The presence of multiple resonators leads to a collective behaviour, where the peaks are determined by the resonant frequencies of each resonator. Furthermore, the analytical model was further validated at low frequencies. As depicted in Fig. 4, sound absorption measurements were conducted for normal incidence, employing a 45.0 mm diameter impedance tube, as delineated in reference [33]. In these experiments, a quarter-wave resonator with a duct length tailored to yield a resonant frequency of 110 Hz was utilised. Fig. 5 shows a compelling comparison between the analytical model, represented by the continuous red curve, and the corresponding experimental measurement, depicted by the dashed black curve. The striking congruence between these two trends underscores the good alignment between the predictions generated by the analytical model and the actual experimental outcomes. A subtle frequency shift of 2 % is discernible in the comparison. This displacement can be ascribed to the simultaneous influence of two factors. Firstly, the most prominent factor is the approximation of the equivalent duct length. In the analytical model, a linear duct with a precisely defined length is taken into account, whereas in the coiled duct configuration, the same length is applied to the equivalent pathway along the duct axis. The second factor pertains to potential alterations in the duct dimensions that might arise during the 3D moulding process of the resonator. This validation process at low frequencies serves to bolster the reliability and accuracy of the analytical model in capturing the intricate dynamics of the quarter-wave resonators.

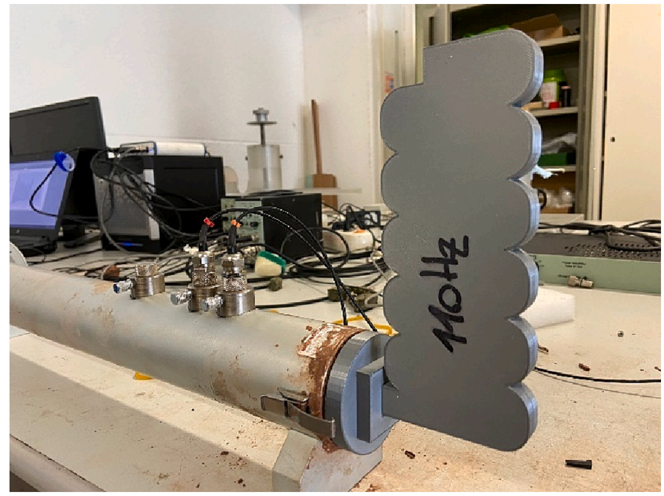

Fig. 4. Normal incidence sound absorption coefficient – experimental measurement setup according to standard.

Furthermore, the dissipation characteristics are influenced by the perforation ratio, which refers to the ratio between the cross-sectional area of the tube and the unit cell area. Increasing the perforation ratio can enhance the acoustic damping capacity of the metamaterial. Previous experimental studies [31,32,43] have demonstrated that the perforation ratio affects the level of damping, resulting in three distinct regimes: under-damping, optimal damping, and over-damping. Under-damping occurs when the system has insufficient damping, leading to incomplete absorption at resonant frequencies. Optimal damping refers

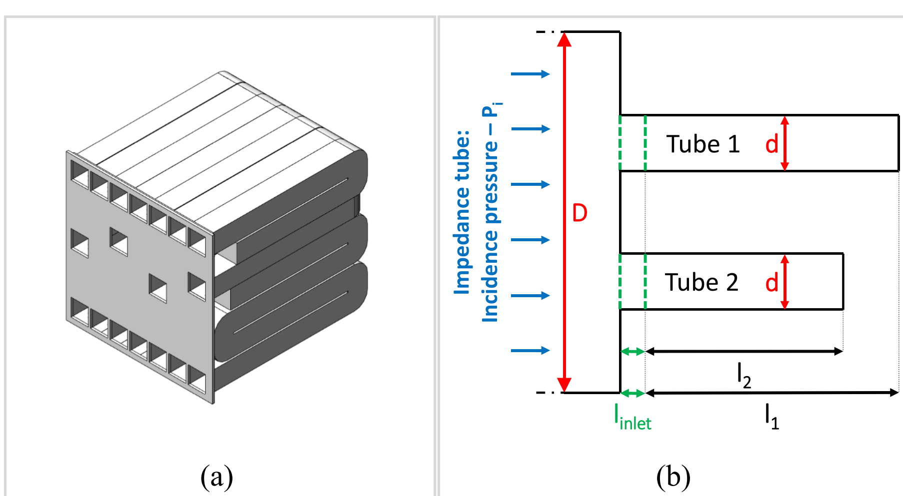

Fig. 3. (a) A 3D of 18 quarter-wave resonators in parallel, (b) schematic representation of the system of two quarter-wave resonators in parallel.

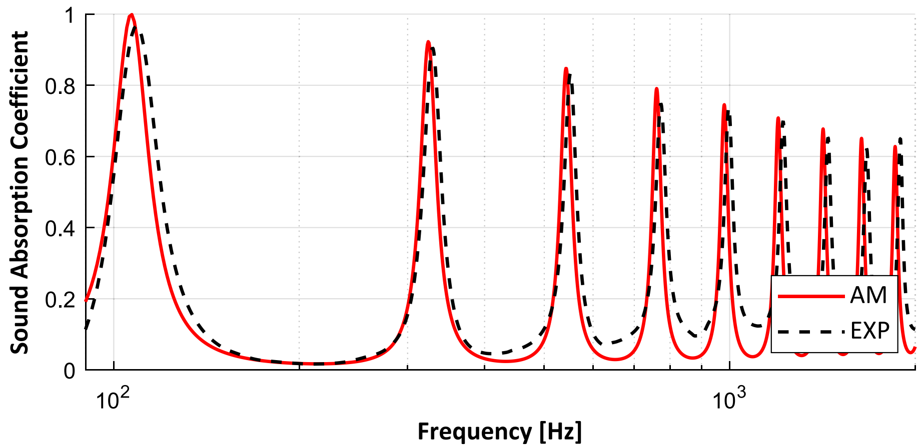

Fig. 5. Normal incidence sound absorption coefficient – comparison between analytical (AM – solid red line) and experimental measurements (EXP – dashed black line).

to a balanced damping level that maximises absorption performance within the desired frequency range. Over-damping happens when the system is excessively damped, leading to reduced absorption and a wider bandwidth. Therefore, the perforation ratio is a crucial factor in achieving the desired acoustic damping characteristics, and their optimisation is necessary to achieve the desired broadband sound absorption behaviour.

Thus, summarising the acoustic behaviour of these resonators is influenced by two main geometric parameters. Firstly, the length l of the duct determines the resonant frequency at which the absorption peak and subsequent higher-order harmonics occur, as described by Equation (1). Secondly, the porosity of the system, which represents the ratio of the inlet section of the duct (corresponding to the "empty" area) to the section of the specimen in which it is inserted (corresponding to the "solid" area), affects the damping of the resonator and, consequently, the amplitude of the absorption peak. Fig. 6 illustrates this aspect, where the resonator length l is kept constant at a resonant frequency of 100 Hz, and the side length of the duct section d is varied within the range of [0.011 – 0.045] m, resulting in a change in the perforation ration ϕ_{sec}. It can be observed that the absorption amplitude increases as the side length of the duct section increases, reaching a maximum value at 0.04 m, and then decreases again.

This behaviour highlights the importance of selecting appropriate geometric parameters for achieving the desired absorption performance. By optimising the resonator length and the porosity of the system, it is possible to enhance the absorption characteristics of the coiled-up quarter-wave resonators, particularly in the low-frequency range.

2.1. Geometric optimisation process: General design considerations

The procedure adopted in the study aims to achieve excellent broadband sound absorption while limiting the thickness of the metamaterial: all steps are schematically shown in Fig. 6.

Fig. 7 illustrates an example of the above procedure. Ten resonators, logarithmically spaced within the frequency range from f_{min} of 100 Hz to $3{\cdot}f_{min}$, delineated here by blue dashed lines, are depicted in grayscale. The red curve illustrates the trajectory of the global absorption coefficient, derived from the envelope of the ten resonators arranged in parallel.

In the context of an absorber designed to operate within a specific octave band, when compared to the optimisation procedure defined for the broadband system, there is a reduction in the frequency range over which the n resonators are effectively coupled in parallel. Specifically, we observe that given the central frequency of the designated band f_c, the limits for f_{min} and f_{max} are established in accordance with Equation (7). Consequently, the frequency interval for accommodating n parallel resonators spans from f_{min} to f_{max}, where f_{max} equates to twice f_{min}.

$$f_c = f_{min}\cdot\sqrt{2} = \frac{f_{max}}{\sqrt{2}}, \tag{7}$$

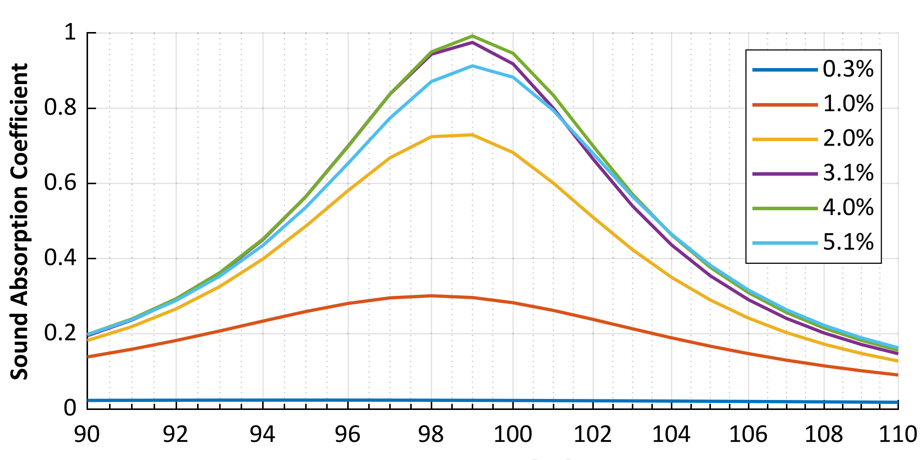

Fig. 6. Amplitude of absorption coefficient for normal incidence as the perforation ration ϕ_{sec} changes (100 Hz resonator with a specimen cross section of 0.2 × 0.2 m).

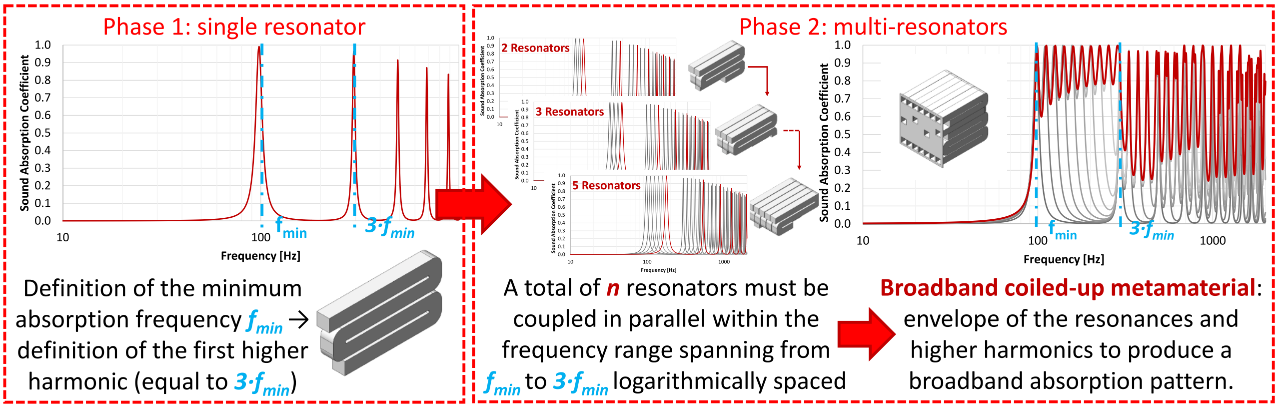

Fig. 7. Design procedure for a broadband coiled-up metamaterial.

Fig. 9 illustrates the dimensioning procedure for an absorber centred in the 250 Hz octave band. Similar to Fig. 8, ten resonators (depicted in grayscale) were logarithmically spaced between f_{min} of 177 Hz and $2{\cdot}f_{min}$. The design frequency range was adjusted in accordance with Equation (7), with the overall absorption emphasised in red, representing the result obtained from the envelope of the ten individual curves.

Once both the analytical model describing the acoustic behaviour and the design procedure have been established, the various interactions between the individual geometrical parameters and the acoustic absorption coefficient for normal incidence were analysed, evaluating how to modify the geometry of the metamaterial in order to have the best system in terms of both absorption efficiency and overall dimensions. Trying to extend as far as possible the considerations that have arisen from the specific geometries presented, some guidelines are extrapolated that may help in the design of a metamaterial for broadband absorption, an aspect that is rarely treated and reported in the literature.

To achieve this, a comprehensive analysis was undertaken. Within this analysis, a metamaterial was considered with a fixed front surface dimension of $D = 0.20$ m and a consistent total thickness of 0.20 m, while simultaneously varying the number of ducts n coupled in parallel and the side length d of the square duct inlet section. The geometric dimensions related to both the frontal surface area of the metamaterial and its thickness were determined while considering materials commonly employed in the civil sector, thus taking into consideration potential practical applications. It is worth noting that, in the scenario of an absorber with an f_{min} of 100 Hz and, consequently, a straight duct length of 0.858 m, the ability to confine the entire structure within a maximum thickness of 0.20 m would result in a reduction of overall dimensions by approximately one-fifth.

Fig. 10 illustrates a colour-coded map depicting the average value of the sound absorption coefficient for normal incidence, computed across

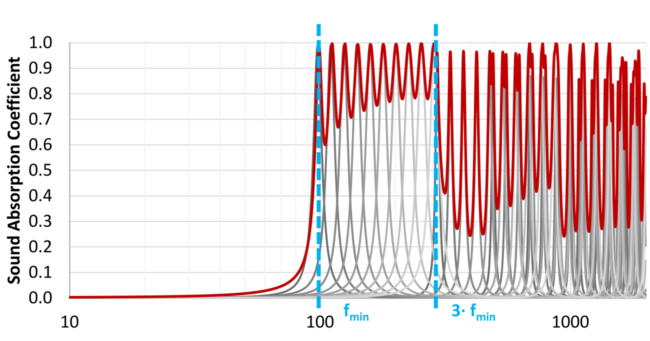

Fig. 8. Normal incidence sound absorption measurements of ten single resonators (grayscale curves) and of the broadband parallel system (red solid line).

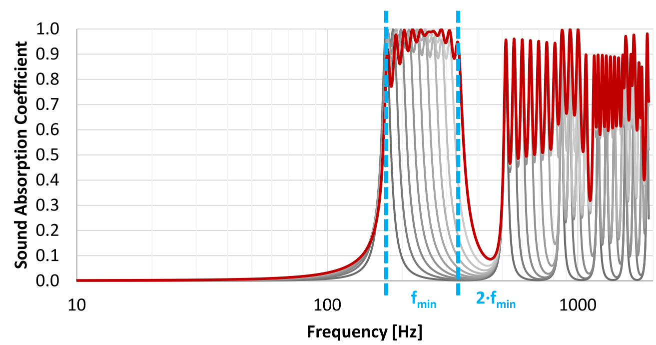

Fig. 9. Normal incidence sound absorption measurements of ten single resonators (grayscale curves) and of the octave band parallel system (red solid line).

a frequency range spanning from 90 Hz to 2000 Hz. The analysis is conducted on a metamaterial with a minimum absorption frequency $f_{min} = 100$ Hz, consequently the ducts are spaced logarithmically up to a maximum frequency of $3{\cdot}f_{min} = 300$ Hz, which is necessary to obtain a broadband absorber as explained at the beginning of this section. The depicted section of the graph only includes feasible geometric configurations, where the total surface area of the ducts is smaller than the frontal surface area of the hosting metamaterial. This delineation is crucial as it defines the limits within which workable metamaterial configurations can be designed and constructed. Furthermore, the black dot represents the optimised geometry (which will be presented later), which exhibits an average absorption coefficient exceeding 0.7. The selection of this combination of the number of ducts n and their side cross-section d, leading to an average absorption of 0.7 and not exceeding it, was made while consistently considering the overall system dimensions. These dimensions account for the minimum thickness required for the ducts to be viable and the thickness limitation imposed on the entire system.

From the observations drawn from Fig. 10, several general design considerations can be made for metamaterials that utilise the parallel coupling of quarter-wave resonators to achieve broadband absorption:

- keeping the side of the duct cross-section d constant and increasing the number of ducts n results in higher sound absorption coefficients for normal incidence.
- As the number of ducts n increases, the available space for coiling the ducts reduces. This decrease in available space causes an increase in the overall size of the absorber, particularly in terms of its total thickness.

Considering these insights, designing such a system involves striking a balance between the absorption efficiency of the metamaterial,

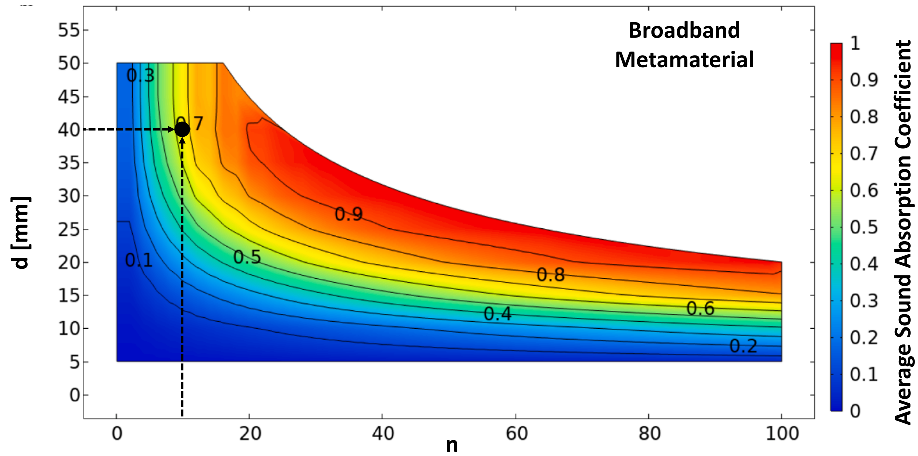

Fig. 10. Average sound absorption coefficient – design map for a broadband metamaterial with a square-section side equal to D = 0.2 m and a f_{min} = 100 Hz.

quantified by the absorption amplitude, and the physical constraints, particularly concerning the available thickness for accommodating the ducts: to facilitate this balance, the presented map in Fig. 10 offers a versatile tool for designing absorbers of various sizes while maintaining a desired average absorption coefficient.

Certainly, the same principles and considerations for design can be extended to octave band absorbers as well. Fig. 11, similar to Fig. 10, demonstrates the average absorption coefficient map, but for an octave band absorber designed to operate in the 250 Hz frequency range. The number of parallel ducts n and the side of the inlet section d are represented on the abscissa and ordinate, respectively. The average coefficient is calculated over the specified frequency range [157 Hz – 375 Hz]. This map allows you to understand how variations in these parameters affect the acoustic performance of the metamaterial within the specific octave band. The black dot represents the optimisation geometry that will be presented in Section 2.3, with the geometric parameters in Table 3.

The maps in Fig. 10 and Fig. 11 are designed specifically for the given frequency ranges (broadband absorption from 100 Hz to 300 Hz in Fig. 10 and octave band absorption around 250 Hz in Fig. 11). As you decrease the minimum frequency f_{min} or select different octave bands, the resonant frequencies of the quarter-wave resonators and their interactions will change. Therefore, these maps will not be directly applicable to different frequency ranges.

Table 2
Optimisation geometry – broadband metamaterial with double parallel resonators.

Total thickness [m]	D [m]	d [m]	n [-]	$Fc_{\lambda/4}$ [Hz]	l_{tot} [m]
0.200	0.200	0.028	9 × 2 = 18	100.0	0.858
				113.0	0.759
				127.7	0.672
				144.2	0.595
				162.9	0.527
				184.1	0.466
				208.0	0.412
				235.0	0.365
				265.5	0.323

2.2. Geometric optimisation process: Broadband coiled-up metamaterial

In the forthcoming section, we will embark on a more detailed exploration, focusing specifically on the optimisation of a broadband absorber. This optimisation process commences with a prescribed minimum frequency, denoted of f_{min} = 100 Hz, and we will highlight all the challenges encountered while trying to reconcile compact geometric dimensions with optimal acoustic performance. This process, implemented within the Matlab environment [44,45], is schematised in Fig. 12.

When considering the dimensional constraints, the optimised

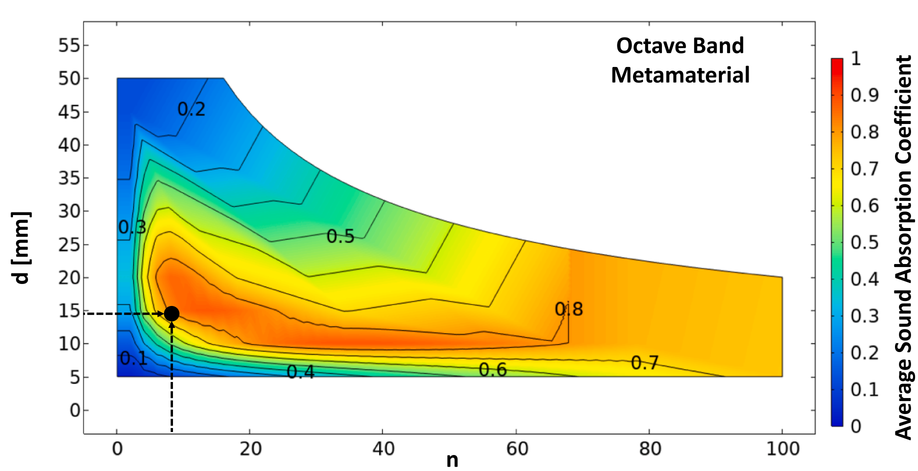

Fig. 11. Average sound absorption coefficient – design map for an active band metamaterial with a square-section side equal to D = 0.2 m and a central frequency band f_c = 250 Hz.

Table 3
Optimisation geometry – 250 Hz octave band metamaterial with 8 parallel resonators.

250 Hz octave band metamaterial – 8 parallel resonators					
Total thickness [m]	D [m]	d [m]	n [-]	$Fc_{\lambda/4}$ [Hz]	l_{tot} [m]
0.200	0.100	0.014	8	177.00	0.485
				195.50	0.439
				215.94	0.397
				238.51	0.360
				263.45	0.326
				290.98	0.295
				321.40	0.267
				355.00	0.242

geometry, indicated by the black dot in Fig. 10, possesses the following geometric parameters: the frontal section of the metamaterial with a side length of $D = 0.2$ m, the frontal section of the ducts with a side length of $d = 0.04$ m and a total of $n = 9$ resonators. However, with a total thickness of 20.0 cm that takes into account potential practical applications, this geometry cannot be accommodated within the prescribed physical constraints. The constraints arise primarily from two factors: the side length of the cross-section of the duct d, which defines the amplitude of absorption, and the number of resonators n, which influences the variation in absorption amplitude. Fig. 13 illustrates the trend of the absorption coefficient as the number of resonators n changes: Fig. 13a illustrates a surface plot with consistent metamaterial porosity (characterised by $D = 0.2$ m and $d = 0.04$ m) and a uniform minimum absorption frequency (100 Hz). In detail, the x-axis displays frequency, the y–axis indicates the number n of resonators aligned in parallel across the frequency spectrum under examination and logarithmically spaced (ranging from 100 Hz to the first higher harmonic at 300 Hz), while the colour gradient denotes the extent of absorption. Fig. 13b illustrates the evolution of absorption curves as the number of resonators n varies. Specifically, the curves depict scenarios with 2, 8, 14, and 20 resonators coupled in parallel.

It can be observed that as the number of resonators increases, the envelope of the absorption coefficient becomes less fluctuating. This phenomenon occurs because with more ducts, the absorption peaks occur at frequencies closer together, leading to a more stable and heightened absorption trend. The absorber becomes more efficient due to the multiple ducts working at frequencies in close proximity, thus elevating the average absorption coefficient.

In summary, the number of resonators coupled in parallel has a significant impact on the trend of the absorption coefficient in the metamaterial. In this context, with a given duct section side length $d = 0.04$ m and a front section for the metamaterial $D = 0.2$ m, the upper limit for the number of resonators that can be accommodated amounts to $n = 24$. It's imperative to acknowledge that these resonators can be positioned in parallel solely if they are treated as straight, as there would not be adequate space available to coil them, consequently yielding an absorber that is highly effective yet oversized. Hence, the determination of the suitable value for n, the number of resonators to be integrated, must be predicated on the desired trade-off between absorption efficiency and the maximum overall dimensions of the envisaged system.

Therefore, when attempting to compact the optimised geometry by coiling the channels, it becomes challenging to simultaneously retain the necessary dimensions for achieving effective broadband absorption. Balancing the size constraints imposed by coiling and the requirements for optimal absorption performance is a complex task that needs to be carefully considered during the design process. In an effort to pursue these objectives, an alternative solution was pursued using double resonators. Initially, the side length of the duct section was reduced from $d = 0.040$ m to $d' = 0.028$ m. This reduction was achieved while maintaining the same duct area. In the first case, there is a single duct, while in the second case, there are two resonators of the same length: mathematically, this can be expressed as $d^2 = 2{\cdot}(d')^2$. This approach allows

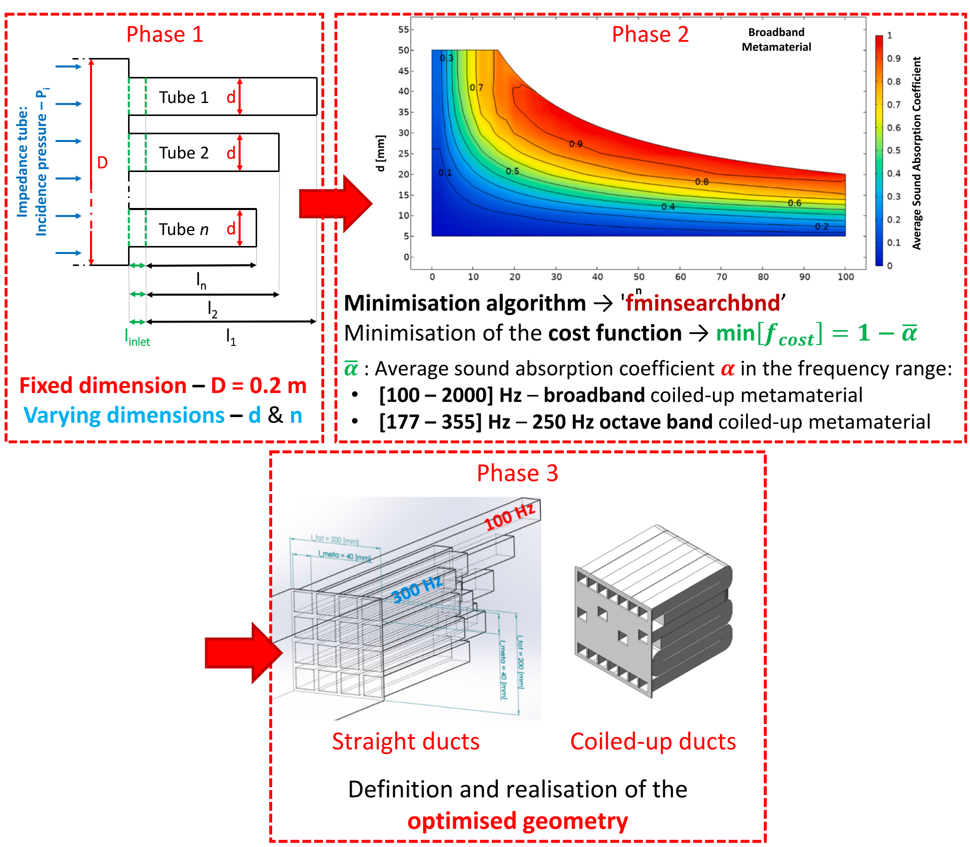

Fig. 12. Outline of the geometric optimisation process.

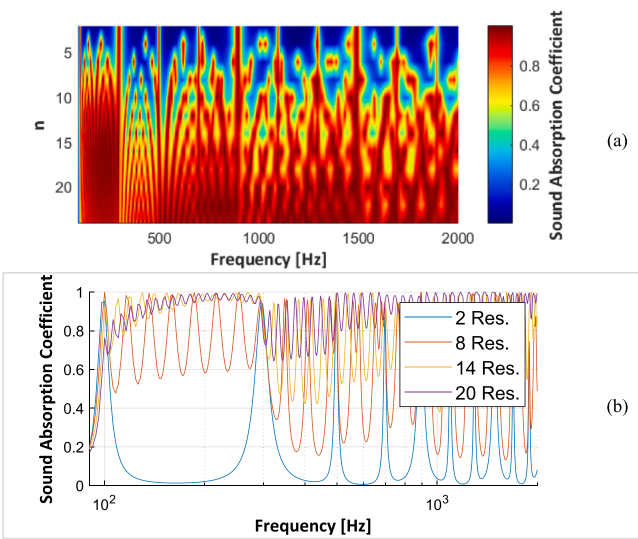

Fig. 13. Influence of the number of resonators n coupled in parallel in the frequency range [100 – 300] Hz: (a) surface plot, (b) sound absorption curves as n varies.

for a reduction in the cross-sectional area of the channels, enabling them to fit within the specified thickness limits due to their slimmer cross-section. Simultaneously, by doubling the number of channels, the ratio between the areas remains constant, preventing a collapse in the absorption amplitude. Consequently, the number of resonators n goes from 9 single resonators to 9 double resonators within the frequency range of 100 – 300 Hz, resulting in a total of 18 resonators when considering the doubled configuration. Therefore, the optimisation geometry of the double-resonator metamaterial has the geometrical characteristics of Table 2, where D is the length of the square-section of the front mask, where there is the incident sound field and where resonators, with the side length of the duct section equal to d, are placed. n is the number of resonators, remembering that there are 9 different resonators which have been doubled to maintain an efficient ratio of full area to empty area. Resonators are logarithmically spaced with the frequencies of column 4, from which the l_{tot} duct lengths in column 5 were determined using the formula in Equation (1).

2.3. Geometric optimisation process: Octave band coiled-up metamaterial

The optimisation analysis was not limited to the study of a broadband metamaterial, recognising that when compactness is a priority, such a design might yield reduced efficiency. As highlighted in the opening section, the central challenge of these systems resides in addressing lower frequencies. To this end, an evaluation of absorbers functioning within specific octave bands was also analysed. These octave band absorbers, operating within narrower frequency spans compared to their broadband counterparts, exhibit heightened efficacy while affording the potential for exceptional compactness. All design considerations are presented in Section 2.1 and illustrated in Fig. 10.

Parallel to the comprehensive study on the broadband absorber, similar analyses were conducted on two metamaterials tuned to octave band absorbers, with central frequencies of 125 Hz and 250 Hz, respectively. Illustrated in Fig. 14, the progression of the absorption coefficient for normal incidence is charted against varying counts of absorbers. This portrayal is pertinent to both the 125 Hz octave band absorber (Fig. 14a) and the 250 Hz version (Fig. 14b).

In contrast to the broadband configuration, the octave band systems demonstrate a reduced demand for resonators to attain notable efficiency. With merely 10 resonators, the absorption amplitude spans from 0.7 to 1.0 for the 125 Hz absorber and from 0.8 to 1.0 for the 250 Hz counterpart. Additionally, an intriguing aspect emerges: as f_{min} escalates, given a constant number of resonators n, the system can be further compacted. This is attributed to the fact that higher f_{min} values correspond to shorter duct lengths, consequentially diminishing the total thickness of the system.

To execute experimental measurements in accordance with the stipulated standard [33], leveraging an impedance tube already housed within the acoustics laboratory at the University of Ferrara, a geometry optimisation was undertaken. Specifically, an absorber was optimised for operation within the 250 Hz octave band. Notably, the absorber was tailored to possess a circular cross-section equal to the diameter of the measurement tube itself, measuring 100.0 mm. This optimised absorber configuration encompasses the incorporation of 8 resonators, coupled in parallel. To provide a comprehensive view, the key geometrical parameters of this optimised setup are presented in Table III, where D is the diameter of the front mask, where there is the incident sound field and where resonators, with the side length of the duct section equal to d, are placed. n is the number of resonators coupled in parallel. The resonators are logarithmically spaced with the frequencies of column 4, from which the l_{tot} duct lengths in column 5 were determined using the formula in Equation (1). The comparison curves between the analytical model and the finite element model will be presented in Section 3.

3. Experimental validation

3.1. Prototype realisation

Using the analytical model, the optimisation geometry of the double-resonator metamaterial was defined, which has the geometrical characteristics of table 2. The fabrication of the 3D prototype of the metamaterial, shown in the CAD drawing in Fig. 16a for the broadband metamaterial and in 16c for the octave band material, was done by 3D printing, using the Original Prusa i3 MK3S + 3D printer with PLA plastic

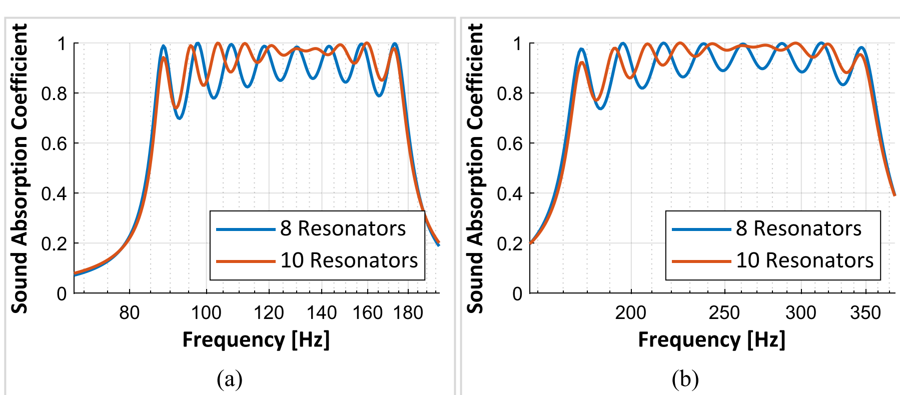

Fig. 14. Influence of the number of resonators n coupled in parallel for octave band absorbers: (a) 125 Hz octave band absorber, (b) 250 Hz octave band absorber.

material. All ducts were moulded by dividing them into two half-shells so as to avoid supporting materials, which are difficult to remove (Fig. 15b and c). In each half-shell, a male–female coupling system was made so as to ensure the correct union between the two halves and to avoid leakage inside the duct as much as possible, making the acoustic behaviour of the resonator totally inefficient. For the same purpose, the two halves were joined using glue and held together in a press for at least 12 h. Following multiple tests, it was observed that altering the percentage of wall filling did not affect the acoustic performance of the ducts. Consequently, a 20 percent fill was chosen for printing the solid components of the geometry. This observation underscores that the primary concern is the connection between the two halves forming the moulded ducts. It is imperative to exercise utmost care during the gluing process to prevent any leakage. Once the 18 resonators are printed, they are placed in parallel within the front mask to compose the final metamaterial, as shown in Fig. 15a.

The same procedure was employed for the fabrication of the optimised metamaterial for the 250 Hz octave band, with the corresponding geometric dimensions listed in Table 3. Fig. 16 depicts photographs of the two fabricated and tested metamaterials. Specifically, Fig. 16a shows the CAD of the broadband metamaterial with the real prototype in Fig. 16b, while Fig. 16c and d features the one designed for the octave band.

3.2. Measurement setup

To measure the optimised metamaterial, a customised measurement tube was designed and fabricated in accordance with the guidelines outlined in the standard [33]: it has a lower limit measurement frequency of $f_{min} = 50$ Hz and an upper limit frequency of $f_{max} = 1000$ Hz.

The tube was made of transparent acrylic (Fig. 17a), which has an inner square section with a side length of D = 0.2 m, thickness of 0.01 m and total length of $l_{tot} = 1.5$ m. On the axis of the upper surface, 3 holes, spaced by a minimum amount of $s_{min} = 0.05$ m, were drilled and the 2 microphones needed to perform the measurement were placed inside them. The sound source is placed at one end of the tube, while the material to be tested is placed at the opposite end. The material is sealed at the side edges using mastic, to avoid possible leakage given by the tube-metamaterial coupling.

Fig. 17b illustrates the experimental setup: the sound source (depicted in red) is powered via a sine sweep signal and the calibration of both microphones in amplitude and phase adheres to the directives outlined in the standard [33]. The metamaterial (rendered in blue) is mounted at the terminal opposite the sound source, utilising internal mastic and external tape to mitigate leakage with the impedance tube. Stiffeners (depicted in green) are introduced on the lateral surfaces of the duct. This measure is undertaken to minimise flexural vibrations within the duct, which could potentially induce alterations in the measured sound absorption coefficient.

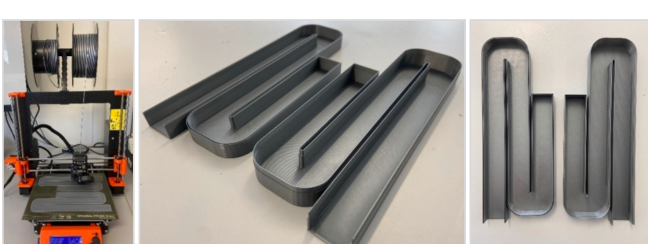

(a) (b) (c)

Fig. 15. (a) 3D printing phase of a resonator; (b + c) two half-shells of a resonators with the male–female coupling system.

3.3. Experimental measurement: Broadband coiled-up metamaterial

With the aim of validating the analytical and numerical model and evaluating the actual acoustic performance of this innovative metamaterial, experimental measurements were conducted to determine the absorption coefficient at normal incidence, according to the ISO 10534–2:2023 standard [33]. This method is based on the fact that the complex reflection coefficient R can be determined by measuring the transfer function H_{12} between two positions, placed at a distance x_1 and x_2 from the test sample. By measuring p_1 and p_2, that is the total pressure in the microphone positions given by the sum of the incident and reflected contributions, we obtain the transfer function H_{12} which represents the entire acoustic field and from this we can calculate the surface impedance, the reflection coefficient and finally the sound absorption as $\alpha = 1 - |R|^2$. Using the sizing formulas in the standard [33] and the above dimensions of the measuring tube, this is characterised by an experimental frequency interval of $50 < f_{exp} < 1000$[Hz].

Fig. 18 displays the comparison between the curve generated through the analytical model (AM – solid red line) and the experimental curve (EXP – dashed black line). Observing the amplitude, it is evident that the experimental curve slightly exceeds the analytical trend, indicating a marginally enhanced real absorption capacity of the metamaterial. Regarding frequency, a minor shift exists between the two trends, presumably attributed to potential imperfections that might arise during the 3D printing process. This manufacturing technique, while effective, might not exhibit the highest precision in terms of dimensional tolerances [46]. Collectively, it can be asserted that a commendable alignment exists between the two curves, confirming the predictions provided by the analytical model. In this case, the frequency shift between the analytical model and experimental data at the first absorption frequency is 1.1 %.

The proposed system exhibits significant drops in the absorption coefficient trend. This is primarily due to the necessity of limiting the number of ducts n to adhere to the predetermined maximum thickness of 20.0 cm, in conjunction with the choice of setting a minimum absorption frequency of 100 Hz. As the value assigned to f_{min} increases, the required length of the ducts decreases, following an inverse proportionality relationship as defined in Equation (1). For instance, transitioning from an f_{min} of 100 Hz to 200 Hz results in a reduction of the maximum duct length from 0.858 m to 0.429 m. This leads to solutions that can either be more compact with the same number of resonators or maintain the same thickness while incorporating more ducts in parallel, thus achieving greater sound absorption efficiency. Fig. 19 illustrates this aspect well by presenting a metamaterial with $f_{min} = 200$ Hz. It shows both the solution analogous to the 100 Hz metamaterial, with 9 resonators in parallel (duct section side $d = 0.04$ m) and the solution with an additional 5 resonators.

3.4. Experimental measurement: Octave band coiled-up geometry

The same measurement procedure was employed to assess the performance of the optimised metamaterial within the 250 Hz octave band. The sole deviation from the measurement setup used for the broadband metamaterial lies in the impedance tube. As elucidated in section 2.3, this absorber was designed for evaluation within an impedance tube situated within the acoustic laboratory of the University of Ferrara. Notably, this impedance tube boasts a circular internal cross-section with a diameter of 100.0 mm. Additionally, a distinct sound source was chosen, designed specifically to be placed in the front of the tube, as illustrated in Fig. 20.

Fig. 21 presents the comparative analysis between the analytical model (AM – solid red line) and the experimental curve (EXP – dashed black line). The same observations can be drawn here as those articulated for the broadband metamaterial, encompassing both the absorption amplitude (slightly elevated in the experimental outcome) and the

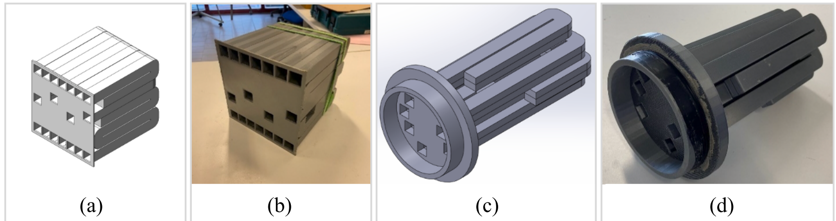

Fig. 16. Measurement prototypes: (a) broadband coiled-up metamaterial; (b) 250 Hz octave coiled-up band metamaterial.

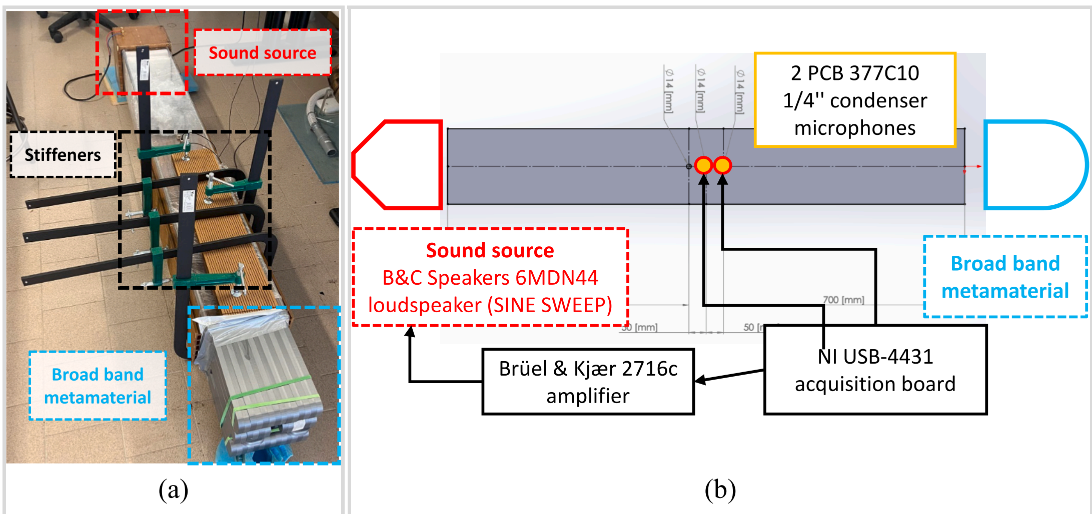

Fig. 17. (a) Measuring impedance tube; (b) measurement set-up with the broadband metamaterial.

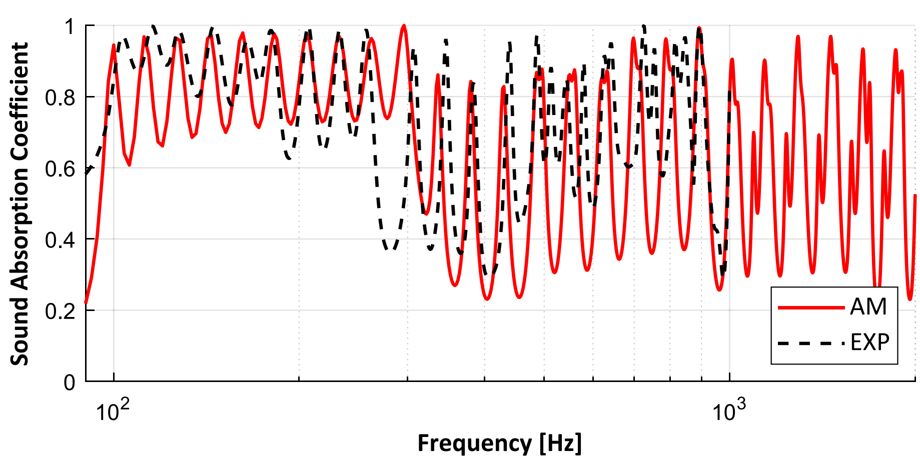

Fig. 18. Normal incidence sound absorption coefficient optimisation geometry with 9 double parallel resonators – comparison between the analytical model (AM – solid red line) and experimental data (EXP – dashed black line).

frequency shift. The degree of agreement remains highly satisfactory, reaffirming the predictive capabilities of the analytical model.

Notably, while the metamaterial's primary design objective revolves around sound absorption within the 250 Hz octave band, it is essential to acknowledge the presence of duct higher-order harmonics, which result in a form of residual absorption at higher frequencies. This phenomenon is chiefly attributed to the optimisation of these higher harmonics within the confines of the particular octave band, thereby mitigating their impact on absorption amplitudes beyond the designated frequency range.

4. Conclusion

An endeavour was undertaken to explore the prospects of achieving an efficient broadband absorber by devising metamaterials composed of multiple quarter-wave resonators while simultaneously striving to curtail overall thickness. Beginning with the analysis of individual resonators, an analytical model was formulated to predict the acoustic behaviour of these entities when coupled in parallel configurations. Initiating with the definition of losses within the individual duct, the separation of the inlet's contribution, modelled as an equivalent fluid using the JCA model, from the thermo-viscous losses at the duct walls, modelled with the Narrow Region model, is undertaken. Utilizing the

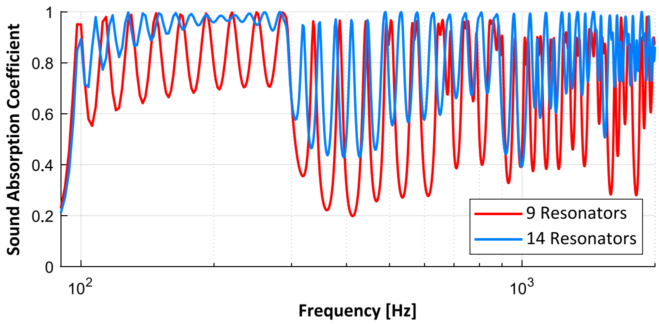

Fig. 19. Normal incidence sound absorption coefficient for a broadband absorber with $f_{min} = 200$ Hz – comparison between 9 resonators in parallel (solid red line) and 14 resonators (solid blue line).

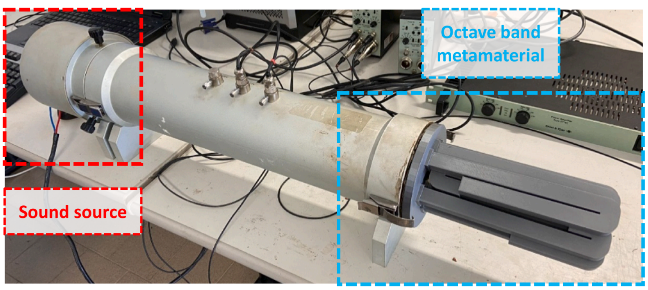

Fig. 20. Measuring impedance tube: measurement set-up with the octave band metamaterial.

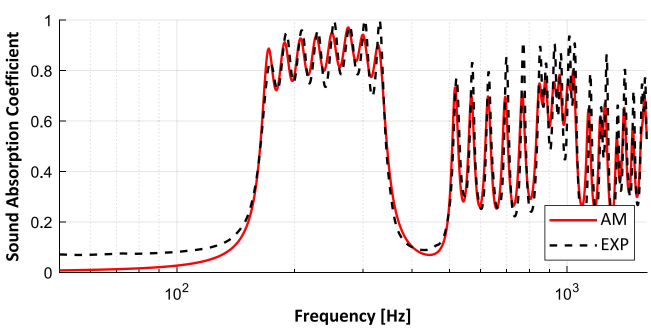

Fig. 21. Normal incidence sound absorption coefficient optimisation geometry 250 Hz octave band – comparison between analytical model (AM – solid red line) and experimental data (EXP – dashed black line).

theory of series and parallel impedances, the total system impedance and normal incidence absorption coefficient were determined, facilitating a systematic exploration of absorption effects by varying geometric parameters.

This exploration resulted in the construction of comprehensive maps and the derivation of design guidelines, contributing to a relatively unexplored area in existing literature. Optimized geometries for both broadband and octave-band metamaterials were fabricated via 3D printing, with polylactic acid utilized as the plastic material. Attention to detail in design and assembly was crucial to avoid potential acoustic performance degradation due to leakage.

Experimental testing within impedance tubes revealed a slight discrepancy between analytical predictions and experimental results, attributed to potential imperfections in the 3D printing process and differences in duct layout between analytical models and CAD designs. Nonetheless, the alignment between analytical and experimental results confirmed the reliability of the analytical model.

In summary, the study showcases the potential of the proposed metamaterial systems as acoustic absorbers, offering customization options for minimum absorption frequency, broadband absorption, and adaptability to various geometries and dimensions. The possibility of "coiling up" channels allows for considerable reduction in overall dimensions, with approximately one-fifth reduction achieved in this study compared to straight-line lengths associated with minimum absorbing frequencies. This research not only contributes to the advancement of metamaterial-based acoustic absorbers but also underscores the efficacy of analytical modeling in designing and optimizing such systems.

CRediT authorship contribution statement

Cristina Marescotti: Writing – original draft, Validation, Software, Methodology, Investigation, Formal analysis, Data curation. **Francesco Pompoli:** Writing – review & editing, Supervision, Resources, Project administration, Funding acquisition, Conceptualization.

Declaration of competing interest

The authors declare that they have no known competing financial interests or personal relationships that could have appeared to influence the work reported in this paper.

Data availability

Data will be made available on request.

Acknowledgements

This research was funded by Ministero dell'Istruzione dell'Università e della Ricerca (Italy), within the framework of the project PRIN 2017, grant number 2017T8SBH9: "Theoretical modelling and experimental characterisation of sustainable porous materials and acoustic metamaterials for noise control."

References

[1] Arenas JP, Crocker M. Recent trends in porous sound-absorbing materials. Sound Vib 2010;44(7):12–7.
[2] Yang J, Lee JS, Kim YY. Metaporous layer to overcome the thickness constraint for broadband sound absorption. J Appl Phys 2015;117(17):174903. https://doi.org/10.1063/1.4919844.
[3] Peiró-Torres MP, Castiñeira-Ibáñez S, Redondo J, Sánchez-Pérez JV. Interferences in locally resonant sonic metamaterials formed from helmholtz resonators. Appl Phys Lett 2019;114(17):171901. https://doi.org/10.1063/1.5092375.
[4] Cai C, Mak C-M, Shi X. An extended neck versus a spiral neck of the helmholtz resonator. Appl Acoust 2017;115:74–80. https://doi.org/10.1016/j.apacoust.2016.08.020.
[5] Guo J, Zhang X, Fang Y, Fattah R. Manipulating reflected acoustic wave via helmholtz resonators with varying-length extended necks. J Appl Phys 2018;124(10):104902. https://doi.org/10.1063/1.5042152.
[6] Cai C, Mak C-M. Acoustic performance of different helmholtz resonator array configurations. Appl Acoust 2018;130:204–9. https://doi.org/10.1016/j.apacoust.2017.09.026.
[7] Griffin S, Lane SA, Huybrechts S. Coupled helmholtz resonators for acoustic attenuation. J Vib Acoust 2001;123(1):11–7. https://doi.org/10.1115/1.1320812.
[8] Maa D-Y. Potential of microperforated panel absorber. J Acoust Soc Am 1998;104(5):2861–6. https://doi.org/10.1121/1.423870.
[9] Fuchs HV, Zha X. Micro-perforated structures as sound absorbers - a review and outlook. Acta Acoust united Ac 2006;92(1):139–46.
[10] Wang C, Huang L. On the acoustic properties of parallel arrangement of multiple micro-perforated panel absorbers with different cavity depths. J Acoust Soc Am 2011;130:208–18. https://doi.org/10.1121/1.3596459.
[11] Chen J-S, Chen Y-B, Cheng Y-H, Chou L-C. A sound absorption panel containing coiled helmholtz resonators. Phys Lett A 2020;384(35):126887. https://doi.org/10.1016/j.physleta.2020.126887.
[12] Chen C, Du Z, Hu G, Yang J. A low-frequency sound absorbing material with subwavelength thickness. Appl Phys Lett 2017;110(22):221903. https://doi.org/10.1063/1.4984095.
[13] Wu F, Xiao Y, Yu D, Zhao H, Wang Y, Wen J. Low-frequency sound absorption of hybrid absorber based on micro-perforated panel and coiled-up channels. Appl Phys Lett 2019;114:151901. https://doi.org/10.1063/1.5090355.
[14] Li Y, Yan J. Acoustic transmission characteristics based on coiled-up space metamaterials. Appl Acoust 2023;203:109199. https://doi.org/10.1016/j.apacoust.2022.109199.

[15] Li Y, Yan J, Peng Y. International journal of mechanical sciences, multiscale porous with coiled-up channel for low-frequency broadband sound absorption. Int J Mech Sci 2022;232. https://doi.org/10.1016/j.ijmecsci.2022.107622.
[16] Maa D-Y. Design of microperforated plate constructions. Chin J Acoust 1988.
[17] Cavalieri T, Cebrecos A, Groby J-P, Chaufour C, Romero-García V. Three-dimensional multiresonant lossy sonic crystal for broadband acoustic attenuation: application to train noise reduction. Appl Acoust 2019;146:1–8. https://doi.org/10.1016/j.apacoust.2018.10.020.
[18] Ho KM, Cheng CK, Yang Z, Zhang XX, Sheng P. Broadband locally resonant sonic shields. Appl Phys Lett 2003;83:5566–8. https://doi.org/10.1063/1.1637152.
[19] Watanabe K, Fujita M, Tsuruta K. Design of non-circular membranes metasurfaces for broadband sound absorption. Japanese J Appl Phys 2020;59. https://doi.org/10.35848/1347-4065/ab7e3e.
[20] McKay A, Davis I, Killeen J, Bennett GJ. SeMSA: a compact super absorber optimised for broadband, low-frequency noise attenuation. Sci Rep 2020;10. https://doi.org/10.1038/s41598-020-73933-0.
[21] Wu X, Fu C, Li X, Meng Y, Gao Y, Tian J, et al. Low-frequency tunable acoustic absorber based on split tube resonators. Appl Phys Lett 2016;109(4):043501. https://doi.org/10.1063/1.4959959.
[22] Xu Z-X, Meng H-Y, Chen A, Yang J, Liang B, Cheng J-C. Tunable low-frequency and broadband acoustic metamaterial absorber. J Appl Physics 2021;129:094502. https://doi.org/10.1063/5.0038940.
[23] Wang ZH, Hui CK, Ng CF. The acoustic performance of ventilated window with quarter-wave resonators and membrane absorber. Appl Acoust 2014;78:1–6. https://doi.org/10.1016/j.apacoust.2013.09.015.
[24] Coulon J-M, Atalla N, Desrochers A. Optimization of concentric array resonators for wide band noise reduction. Appl Acoust 2016;113:109–15. https://doi.org/10.1016/j.apacoust.2016.06.015.
[25] Dasila S, Krishnamurthy CV, Subramanian V. Metamaterial based miniaturized broadband acoustic absorber. J Appl Phys 2023;133:114901. https://doi.org/10.1063/5.0142650.
[26] X. Peng, J. Ji, Y. Jing, *Composite honeycomb metasurface panel for broadband sound absorption*, J. Acoust. Soc. Am. 144(4), EL255–61, (2018). https://doi.org/10.1121/1.5055847.
[27] Li Y, Yan J, Peng Y. Multiscale porous with coiled-up channel for low-frequency broadband sound absorption. Int J Mech Sci 2022;232:107622. https://doi.org/10.1016/j.ijmecsci.2022.107622.
[28] Wanga Y, Wanga Y, Xu J, Yu H, Zhang C, Ren L. Broadband low-frequency sound absorption by coiled-up space embedded in a porous layer. Appl Acous 2021;182:108226. https://doi.org/10.1016/j.apacoust.2021.108226.
[29] Chen J-S, Chen Y-B, Cheng Y-H, Chou L-C. A sound absorption panel containing coiled helmholtz resonators. Phys Lett A 2020;384(35). https://doi.org/10.1016/j.physleta.2020.126887.
[30] Magnani A, Marescotti C, Pompoli F. Acoustic absorption modeling of single and multiple coiled-up resonators. Appl Acoust 2022;186:108504. https://doi.org/10.1016/j.apacoust.2021.108504.
[31] Park JH, Sohn CH. On optimal design of half-wave resonators for acoustic damping in an enclosure. J Sound Vib 2009;319:807–21. https://doi.org/10.1016/j.jsv.2008.06.049.
[32] Sohn CH, Park JH. A comparative study on acoustic damping induced by half-wave, quarter-wave and helmholtz resonators. Aerosp Sci Technol 2011;15(8):606–14. https://doi.org/10.1016/j.ast.2010.12.004.
[33] ISO 10534-2:2023, *Acoustics – Determination of acoustic properties in impedance tubes. Part 2: Two-microphone technique for normal sound absorption coefficient and normal surface impedance.*
[34] Andersen PR. Modelling of acoustic viscothermal losses using the Boundary element method: from method to optimization. The Technical University of Denmark; 2019. PhD thesis.
[35] Kirchoff G. Über den einfluss der wärmeleitung in einem gase auf due schallbewegung", (the effect of heat conduction in a gas on the movement of sound). Ann Phy 1868;210(6):177–93. https://doi.org/10.1002/andp.18682100602.
[36] Magnani A, Marescotti C, Pompoli F. Acoustic absorption fem modeling of single and multiple coiled-up resonators. Proceedings of the 27th International Congress on Sound and Vibration (ICSV27). 2021.
[37] Atalla N, Sgard F. Modeling of perforated plates and screens using rigid frame porous models. J Sound Vib 2007;303:195–208. https://doi.org/10.1016/j.jsv.2007.01.012.
[38] Chevillote F. Controlling sound absorption by an upstream resistive layer. Appl Acoust 2012;73:56–60. https://doi.org/10.1016/j.apacoust.2011.07.005.
[39] Okuzono T, Nitta T, Sakagami K. Note on microperforated panel model using equivalent-fluid-based absorption elements. Acoust Sci Technol 2019;40:221–4. https://doi.org/10.1250/ast.40.221.
[40] Ruiz H, Cobo P, Dupont T, Martin B, Leclaire P. Acoustic properties of plates with unevenly distributed macroperforations backed by woven meshes. J Acoust Soc Am 2012;132:3138–47. https://doi.org/10.1121/1.4754520.
[41] Guo Y, Allam S, Åbom M. *Acoustical study of micro-perforated plates for vehicle applications,* technical paper in SAE. In: 2009 Noise and Vibration Conference and Exhibition; 2009. https://doi.org/10.4271/2009-01-2037.
[42] Congyun Z, Qibai H. A method for calculating the absorption coefficient of a multi-layer absorbent using the electro-acoustic analogy. Appl Acoust 2005;66:879–87. https://doi.org/10.1016/j.apacoust.2004.10.002.
[43] Laudien E, Pongratz R, Pierro R, Preclik D. Fundamental mechanisms of combustion instabilities: Experimental procedures aiding the Design of Acoustic Cavities. AIAA – Liquid Rocket Engine Combustion Instability 1995;169:377–99. https://doi.org/10.2514/5.9781600866371.0377.0399.
[44] The MathWorks Inc. (2022), *MATLAB version: 9.13.0 (R2022b)*, Natick, Massachusetts: The MathWorks Inc. https://www.mathworks.com.
[45] The MathWorks Inc. (2022), *Optimization Toolbox version: 9.4 (R2022b)*, Natick, Massachusetts: The MathWorks Inc. https://www.mathworks.com.
[46] Ciochon A, Kennedy J, Leiba R, Flanagan L, Culleton M. The impact of surface roughness on an additively manufactured acoustic material: an experimental and numerical investigation. J Sound Vib 2023;546:117434. https://doi.org/10.1016/j.jsv.2022.117434.